Nanoscale

ROYAL SOCIETY OF CHEMISTRY

PAPER

View Article Online
View Journal | View Issue

Cite this: *Nanoscale*, 2022, **14**, 1285

Dissolving microneedle-encapsulated drug-loaded nanoparticles and recombinant humanized collagen type III for the treatment of chronic wound *via* anti-inflammation and enhanced cell proliferation and angiogenesis†

Lin-yu Long, [a] Wenqi Liu,[a] Li Li,[b] Cheng Hu, [a] Shuyi He,[a] Lu Lu,[c] Jian Wang,[d] Li Yang*[a] and Yun-bing Wang *[a]

Nowadays, diabetic chronic wounds impose a heavy burden on patients and the medical system. Persistent inflammation and poor tissue remodeling severely limit the healing of chronic wounds. For these issues, the first recombinant humanized collagen type III (rhCol III) and naproxen (Nap) loaded poly (lactic-*co*-glycolic acid) (PLGA) nanoparticle incorporated hyaluronic acid (HA) microneedle (MN) was fabricated for diabetic chronic wound therapy. As the tailored rhCol III was synthesized based on the Gly483-Pro512 segment, which contained the highly adhesive fragments (GER, GEK) in the human collagen type III sequence, it possessed strong cell adhesion. The mechanical strength of the prepared MN was enough to overcome the tissue barrier of necrosis/hyperkeratosis in a minimally invasive way after being applied in wounds. Subsequently, rhCol III and Nap@PLGA nanoparticles were rapidly released to the wound site within a few minutes. The prepared MN possessed favourable biocompatibility and could effectively facilitate the proliferation and migration of fibroblasts and endothelial cells. Furthermore, the regenerative efficacy of the MN was evaluated *in vivo* using the diabetic rat full-thickness skin wound model. These results illustrated that the prepared MN could accelerate wound closure by reducing the inflammatory response and enhancing angiogenesis or collagen deposition, indicating their significant application value in wound dressings for chronic wound repair.

Received 22nd November 2021,
Accepted 20th December 2021

DOI: 10.1039/d1nr07708b

rsc.li/nanoscale

1. Introduction

As the largest organ in the human body, the skin provides protection against external harmful stimuli (such as pathogens or physical impact) and maintains the stability of the human internal environment.[1] Skin injuries, especially chronic wounds, require expensive long-term treatments and imposes a heavy economic burden on the global medical system.[2] Furthermore, several factors such as population aging, diabetes and obesity cause the prevalence of chronic wounds to continue to rise.[3,4] It is estimated that chronic wounds affect 6.5 million patients and cause more than $25 billion in losses each year in the United States.[1,5,6] Therefore, effective therapeutic strategies for chronic wounds have become urgent issue in the global medical field.

Collagen type III is an extracellular matrix protein,[7] which consists of three identical α1 chains and provides elasticity and support for the skin and some hollow organs (such as arteries, uterus, and intestines).[8–10] During the past few decades, due to its easy accessibility, low price and good interaction with cells, collagen type III has been widely used in biomedical fields, such as cosmetics, wound healing and artificial blood vessels.[10,11] In the initial stage of the wound healing process, collagen type III secreted by fibroblasts forms the provisional matrix and guides the fibroblasts and inflammatory cells into the wound site.[12,13] Furthermore, collagen type III may regulate the synthesis of type I collagen,[14,15] accelerates collagen fibrillogenesis and modulate the structural/functional property of the fibrils.[16,17] However, currently commercialized collagen is mainly derived from animal tissues, which leads to the clinical application limits of collagen, such as poor solubi-

[a]*National Engineering Research Center for Biomaterials, Chuanda-Jinbo Joint Research Center, Sichuan University, Chengdu, 610064, China. E-mail: yanglisc@scu.edu.cn, yunbing.wang@scu.edu.cn*
[b]*Institute of Clinical Pathology, West China Hospital of Sichuan University, Chengdu, 610041, China*
[c]*Key Laboratory of Medical Molecular Virology (MOE/NHC/CAMS), School of Basic Medical Sciences and Shanghai Public Health Clinical Center, Fudan-Jinbo Joint Research Center, Fudan University, Shanghai, 200302, China*
[d]*Shanxi Jinbo Bio-Pharmaceutical Co., Ltd, Taiyuan, 030032, China*

†Electronic supplementary information (ESI) available. See DOI: 10.1039/d1nr07708b

lity, batch-to-batch variation in quality and purity, and pathogenic contamination.[18,19] Nowadays, proteins and peptides that resemble endogenous molecules for therapeutic purposes can be obtained through recombinant DNA, protein and peptide engineering, and tissue culture techniques, thereby minimizing the immune response.[18,20] In addition, the recombinant humanized collagen type III (rhCol III) possesses the features of good solubility and strong cell adhesion.[9] At present, rhCol III has been used for myocardial repair, treatment of vaginal atrophy and other biomedical fields.[21,22] But as far as we know, there are no relevant reports about the effect of rhCol III on wound healing. Herein, we systematically researched the full sequence of human collagen type III and screened out the Gly483-Pro512 segment that retained the high cell adhesion fragments (GER, GEK) in the full sequence of human type III collagen through computer-assisted screening.[23] A tailored rhCol III with strong cell adhesion was synthesized based on this segment.

Additionally, it is a commonly used strategy to promote chronic wound healing by inhibiting the inflammatory response to relieve the persistent inflammatory response.[24–28] Naproxen (Nap), a non-steroidal anti-inflammatory drug, has antipyretic, analgesic and anti-inflammatory effects.[29] Nap can be delivered locally to reduce the inflammatory response of the tissue around the wound,[30] and to avoid adverse side effects caused by oral routes or intravenous administration, such as gastrointestinal mucosal irritation and ulcers, nausea and systemic toxicity.[29,31] However, the bioavailability of Nap is limited by its low solubility.[32,33] Topical application of the drug requires frequent removal and reapplication of the dressing, which may severely aggravate acute wounds. A feasible solution is to encapsulate Nap with carriers such as nanoparticles, so that the drug can be continuously released into the wound site for a long time, thereby eliminating the need for frequent dressing changes and reducing inflammation during wound healing.[30]

Moreover, although conventional pharmaceutical dosage forms such as solutions, fiber mats and hydrogels can absorb wound exudate and prevent wound infection to some extent, their poor retention in the wound site may result in low drug bioavailability, high risk of wound adhesion and frequent replacement required.[2] The traditional dosage forms cannot overcome the tissue barrier of necrosis/hyperkeratosis and the presence of significant exudate production in chronic wounds, making it difficult for the drug to penetrate the wound bed.[2,34] Microneedle (MN), consisting of arrays of micro-scale needles, is commonly used for topical transdermal delivery of various therapeutic molecules by creating transport pathways through the skin without damaging neurons in the dermis.[35–40] Recently, MN has been proven to overcome the tissue barrier and penetrate into a microbial biofilm,[41] thus accurate doses of the therapeutic agents, including mesenchymal stem cells, antibiotics, vascular endothelial growth factor, oxygen and so on, can be effectively and painlessly delivered to the wound bed.[2,42–48] It is worth mentioning that the MN is minimally invasive, thereby inducing minimal pain and inflammation compared to other invasive methods.[49–51] Furthermore, some bio-inspired adhesive MN can suture wounds through mechanical interlocking and deliver drugs to the wound beds at the same time.[52,53] Therefore, MN is considered to be one of the optimum choices to deliver the Nap-loaded nanoparticles and rhCol III for chronic wound therapy. However, research on the application of MN to deliver anti-inflammatory drugs and therapeutic protein macromolecules in the treatment of chronic wounds is still rare, and their actual effects remain to be explored.

Herein, in order to produce a clinically translatable dressing for wound healing, first, rhCol III and Nap-loaded poly (lactic-*co*-glycolic acid) (PLGA) nanoparticles-incorporated hyaluronic acid (HA) MN was fabricated for diabetic chronic wound therapy (as shown in Fig. 1). As shown in Fig. 1, such MN was fabricated by a template-molding method and was composed of dissolvable HA, which was the main component of the skin extracellular matrix.[54] After application to the wound, the pyramid-shaped needle tip helped to insert the drug-loaded needles easily into the wound bed with minimal collateral tissue damage. Subsequently, with the dissolution of MN, rhCol III and Nap@PLGA, nanoparticles were rapidly released to the wound site within a few minutes. We proved that the prepared MN could promote the proliferation and migration of two types of cells (fibroblasts and endothelial cells) that were critical to the wound healing process. Finally, the ability of MN to promote chronic wound healing was determined *in vivo* by using the diabetic rat full-thickness skin wound model. In conclusion, this research is expected to provide an effective novel treatment for diabetic chronic wound therapy and prove the effectiveness of the tailored rhCol III to promote wound healing.

2. Materials and methods

2.1 Materials

HA (M_w = 10 wt, >99%) was purchased from Qufu Guanglong Biological Products Co., Ltd (Qufu, China). Naproxen (Nap) was purchased from Dalian Meilun Biotechnology Co., Ltd (Dalian, China). Poly(lactic-*co*-glycolic acid) (PLGA, acid terminated, lactide : glycolide 50 : 50, M_w 38 000–54 000), Nile red, dimethyl sulfoxide (DMSO), and fluorescein isothiocyanate (FITC) were purchased from Shanghai Macklin Biochemical Co., Ltd (Shanghai, China). The recombinant humanized collagen type III (rhCol III) was prepared by Shanxi Jinbo Bio-Pharmaceutical Co., Ltd (Taiyuan, China). rhCol III was composed of 16 tandem repeats of the triple-helix fragment. The tandem repeats peptide contains the sequence of high cytoactive, derived from the Gly483-Pro512 sequence of the human type III collagen.[23] The poly(dimethylsiloxane) (PDMS) micromolds were fabricated by Taizhou Microchip Pharmaceutical Technology Co., Ltd (Taizhou, China).

2.2 Preparation and characterization of Nap-loaded PLGA (Nap@PLGA) nanoparticles

Here, an interfacial deposition method was used to prepare Nap@PLGA nanoparticles.[55,56] Briefly, 2 mg of Nap and 10 mg

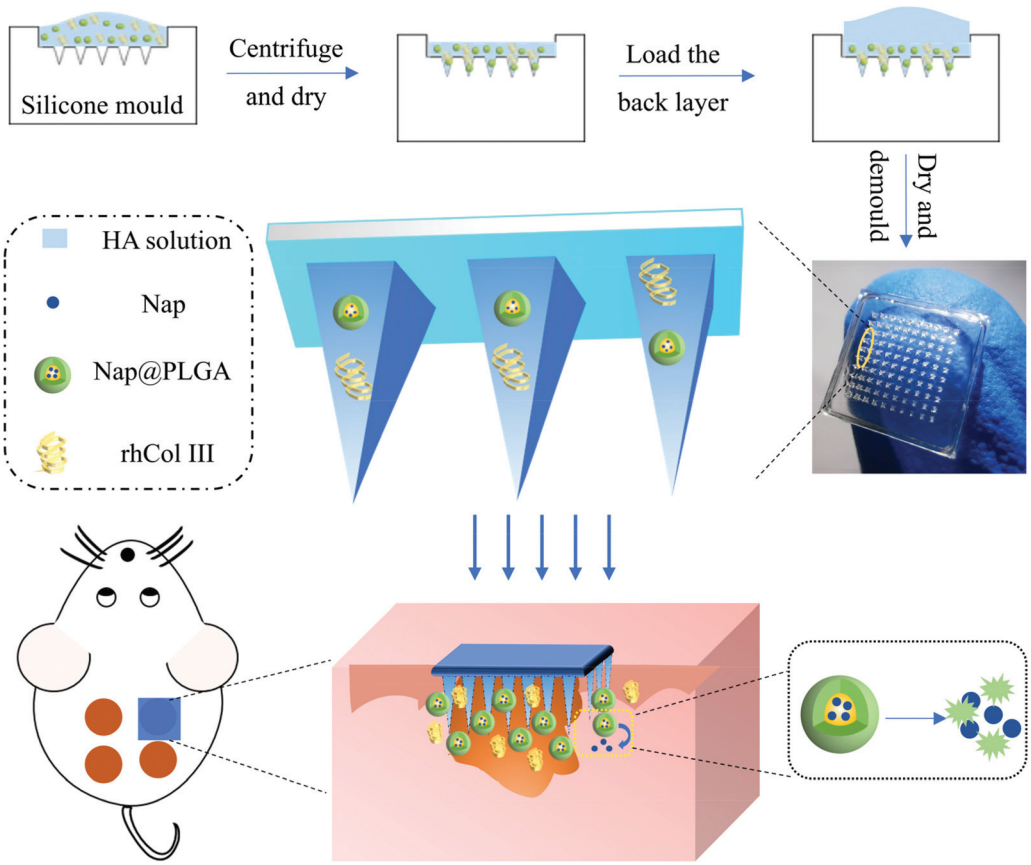

Fig. 1 The fabrication process of rhCol III and Nap@PLGA nanoparticles loaded MN with its application in promoting chronic wound healing.

of PLGA were dissolved in 1 mL of DMSO. Subsequently, the solution was added dropwise into a certain amount of deionized (DI) water with slow stirring. Finally, the mixture was dialyzed in DI water for 3 days. Then, the solution of Nap@PLGA nanoparticles was collected. In addition, 0.1 wt% nile red was used to prepare the fluorescence-labeled PLGA nanoparticles using a similar method as described above.

Size and zeta potential, and the morphology of Nap@PLGA and PLGA nanoparticles (160 μg mL^{-1}, aqueous solution) were determined using dynamic light scattering (DLS, Malvern Zetasizer Nano-ZS90 apparatus, Malvern, U.K.) and transmission electron microscopy (TEM) (Hitachi H-600, Japan), respectively.

2.3 Drug loading and *in vitro* drug release study

Herein, an ultraviolet-visible spectrophotometer (UV-2401PC, Shimadzu) was used to measure the absorbance of the nanoparticle solution (in DMSO) at 332 nm to determine the loading efficiency of Nap. The drug-loading efficiency (LE) and drug-encapsulation efficiency (EE) were calculated as the following equations:

$$\mathrm{LE}\,(\%) = \frac{M_{\mathrm{Nap}}}{M_{\mathrm{Nap}} + M_{\mathrm{PLGA}}} \times 100\% \quad (1)$$

$$\mathrm{EE}\,(\%) = \frac{M_{\mathrm{Nap}}}{M_{\mathrm{added}}} \times 100\% \quad (2)$$

where M_{Nap}, M_{PLGA} and M_{added} are the mass of Nap loaded in the nanoparticles, the mass of PLGA in the formulation and mass of initial added Nap, respectively.

To research the *in vitro* drug release profile of nanoparticles, a dialysis bag (MWCO: 3500 Da) containing 1 mL of Nap@PLGA solutions (1 mg mL^{-1}) was immersed in 10 mL of PBS. At different time points, 1 mL of supernatant was collected and 1 ml of fresh PBS was added. The cumulative amount of Nap released was determined using UV-vis.

2.4 Fabrication of Nap@PLGA and rhCol III co-loaded HA MN

The drug-loaded HA MN was fabricated by a template-molding method. 100 μl of the mixed solution with HA (200 mg ml^{-1}), Nap@PLGA (160 μg ml^{-1}) and rhCol III (500 μg ml^{-1}) was poured into the PDMS mold at first. The needles were filled with the mixture by centrifugation at 3000 rpm for 10 min and dried at room temperature for 24 h. Secondly, another 150 μl HA (200 mg ml^{-1}) solution was poured into the mold and dried at room temperature for 24 h. Finally, the MN-loaded with Nap@PLGA and rhCol III were peeled off from the mold. The control MN, Nap@PLGA-loaded MN, rhCol III-loaded MN

and Nap@PLGA and rhCol III co-loaded MN were named MN-C, MN-Nap, MN-III and MN-III/Nap, respectively.

The fluorescence-labeled MN was prepared by the above method using the nile red@PLGA and FTIC-labeled rhCol III as the model drugs. All the MNs were stored at 4 °C before use.

2.5 Characterization of MN

The appearance of the microneedles was observed with a smartphone with an HD camera (Huawei P30 Pro). Scanning electron microscopy (SEM, S4800, Hitachi, Japan), optical microscopy and a fluorescence microscope were employed to visualize the morphology of the MN. The mechanical property of the MN was evaluated using a universal testing machine (BioTester, 10 N load cell; CellScale, Waterloo, Ontario, Canada). After re-dissolving the prepared MN, the drug loading efficiency of the MN was determined to be 96.49 ± 3.68% (Nap) and 97.24 ± 5.42% (rhCol III) using UV-vis and fluorescence spectrophotometers, respectively. In addition, MN-III/Nap and MN containing FITC-labeled rhCol III were pressed into fresh rat skin for 1 minute, and then pull it out of the skin. An optical microscope and fluorescence microscope were used to observe the skin treated with the MN from different perspectives.

2.6 *In vitro* biocompatibility studies

The biocompatibility of the prepared MNs was conducted by incubating the MN solution with L929 cells or human umbilical vein endothelial cells (HUVECs) *in vitro*. MNs were dissolved in 2 mL complete 1640 cell medium to obtain MN solution. Then, the solution was filtered with a 0.22-micron filter. Additionally, L929 cells or HUVECs were seeded in 96-well plates for 24 h and then co-cultured with 100 μL MN solution for 24 h and 48 h. The CCK8 experiment and cell LIVE/DEAD staining were finally conducted to evaluate the survival rate of the cells and observe the proliferation and morphology of cells.

2.7 Cell scratch experiment

The cell scratch experiment was used to assess the influences of MNs on cell migration. Briefly, 1×10^6 cells were seeded in 6-well plates and incubated at 37 °C (5% CO_2) until they achieved at least 90% confluence. After each well was scratched with a 200 μL pipette tip, the cells were treated with 2 mL MN solution. After incubation at 37 °C (5% CO_2) for 24 and 48 h, microscopic images were taken immediately to observe cell migration. The experiments were repeated three times, and representative images were selected.

2.8 *In vivo* wound healing

All animal procedures were performed in accordance with guidelines for care and use of laboratory animals of Sichuan University and approved by the animal ethics committee of Sichuan University. Firstly, for the purpose of inducing diabetes mellitus type I in rats, a certain amount of streptozotocin solution was injected into SD male rats (70 mg kg^{-1}) through the tail vein. Three days after injection, round full-thickness skin with a diameter of 1.2 cm on the back of the rats were removed to create a cutaneous wound. Then, male SD rats (150 ± 20 g) with diabetes and wounds were randomly divided into five groups with 6 rats in each group. 24 h after surgery, the wounds of the five groups were treated with PBS (pH = 7.4), MN-C, MN-Nap, MN-III and MN-III/Nap, respectively. Each group was subjected to six parallel experiments, and experiments were conducted every other day for a total of three administrations. The residual MN covered on the wound was washed with sterile PBS solution. The rats were euthanized by injecting an overdose of anesthetic on the 7^{th} or 14^{th} day, and the removed wound skin tissue were fixed with 10% buffered formalin for further histological analysis.

3. Results and discussion

3.1 Characterization of Nap@PLGA nanoparticles

Nanoparticles provide various benefits for encapsulated active drugs, such as enhanced drug stability, improved water solubility, and sustained drug release over a period of time to reduce physiological toxicity.[57,58] In this study, Naproxen (Nap) was effectively encapsulated into poly(lactic-*co*-glycolic acid) (PLGA), which has been approved by Food and Drug Administration for parenteral applications,[6] by an interfacial deposition method.[55,56] As shown in Fig. S1,† the mean diameter of Nap@PLGA nanoparticles determined by DLS was 75.80 ± 0.65 nm, while the mean diameter of PLGA nanoparticles was 67.14 ± 0.27 nm (Fig. S2†). In addition, PDI values of PLGA and Nap@PLGA nanoparticles were 0.077 and 0.089, respectively, which indicated a narrow particles size distribution. Furthermore, since carboxylate groups of PLGA could be ionized at neutral pH,[59] the zeta potential of PLGA and Nap@PLGA particles in deionized (DI) water at 25 °C was found to be −18.97 ± 0.30 mV and −19.20 ± 0.30 mV, respectively. The TEM image of the Nap@PLGA nanoparticles showed that particles are spheres, well-dispersed and with the size of 47.29 ± 13.95 nm (Fig. 2A), while the size of PLGA particles was 41.59 ± 8.75 nm (Fig. S3†). The LE and EE of Nap@PLGA nanoparticles determined by the UV-absorbance at 332 nm were 9.7% and around 62.5%, respectively (Fig. 2B). Dehydration of the hydrophilic shell for TEM detection during the preparation of the sample was the main reason for the particle size measured using TEM being smaller than that measured by DLS.[60]

It was necessary to research the release profile of encapsulated Nap from the PLGA nanoparticles owing to fact that insufficient release may decrease the availability and efficacy of drugs.[57] There are mainly two typical degradation/erosion modes for drug release from biodegradable polymer particles. For the drug-loaded PLGA nanoparticles, the mode of drug release involved mainly the bulk erosion system, which provided an initial burst release followed by a zero-order release.[2] In this study, the *in vitro* drug release profile of Nap from nanoparticles was measured for 14 days (Fig. 2C). 42.42 ± 2.19% of Nap was released from PLGA nanoparticles on day 1,

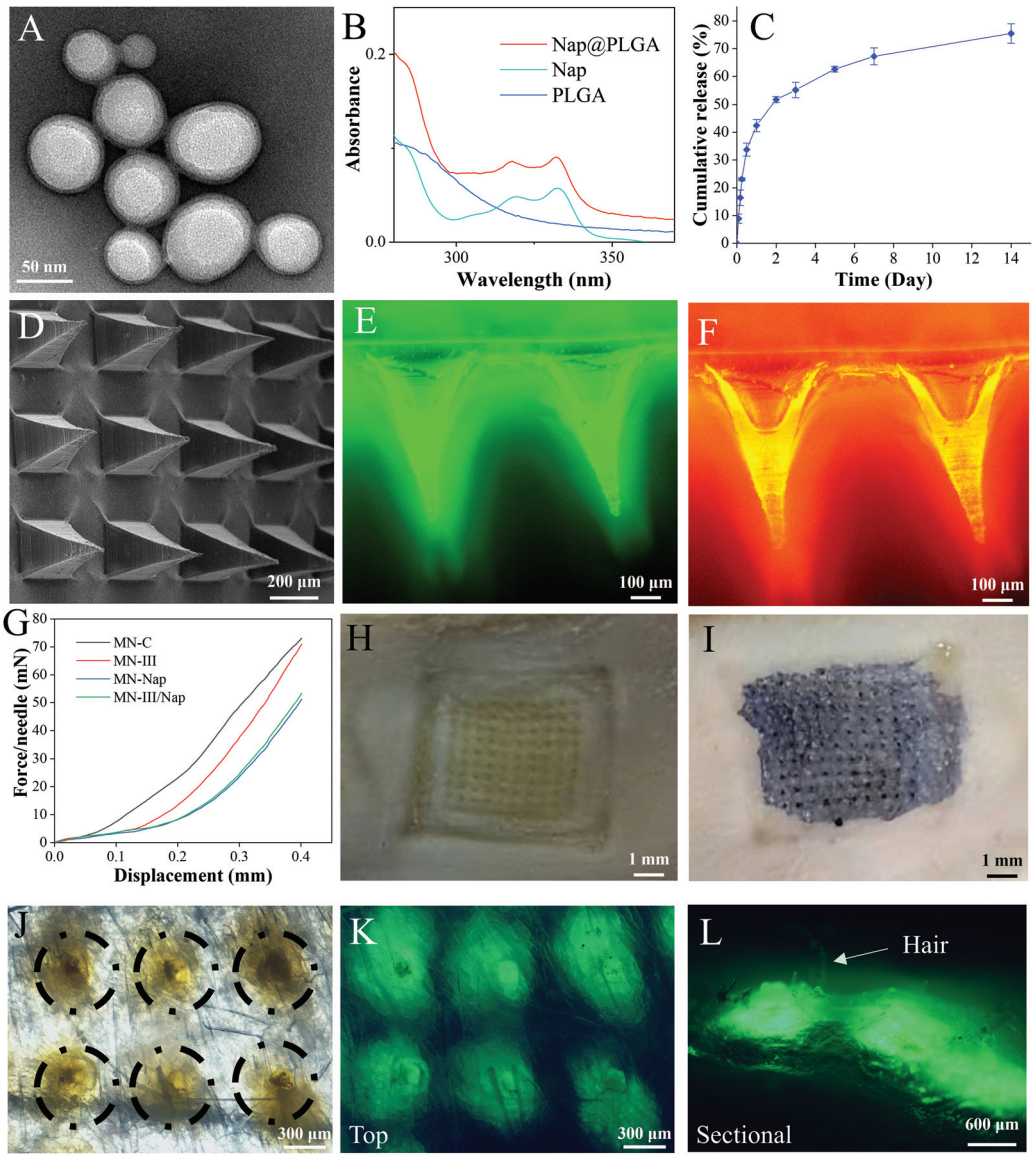

Fig. 2 Characterization of nanoparticles and MNs. (A) The TEM images of the Nap@PLGA nanoparticles in H_2O. (B) UV–vis spectrum of PLGA, Nap, and Nap@PLGA. (C) The Nap cumulative release of Nap@PLGA nanoparticles. (D) SEM images of the microneedle array. The fluorescence photographs of FITC–rhCol III loaded MN (E) and nile red@PLGA nanoparticles loaded MN (F). (G) Mechanical property characterization of the MN patch. (H) Digital photo of fresh rat skin treated with MN. (I) Digital photo of the rat skin stained with trypan blue after MN-III/Nap application. Fluorescence micrograph of fresh rat skin treated with FITC-labeled rhCol III loaded MN: (J) White light channel; (K) and (L) Green light channel.

while 51.76 ± 1.07% of Nap was released on day 2, indicating that there was an initial burst release and the release after that was approximately sustained. Finally, 75.45% of Nap was released by day 14. The burst release was beneficial to improve the permeability of the drug, while sustained release could release the drug over a longer period of time, thereby, alleviating the inflammatory response in chronic wounds.

3.2 Morphologies and mechanical strength of MN

In a typical experiment, the MN array was fabricated by a two-step micro-molding approach. The resulting patch was arranged in a 10 × 10 microneedle array. As shown in Fig. 2D, each micro-needle possessed a pyramid shape with a height of 600 μm, a tip distance of 600 μm and a base side length of 300 μm, which were fundamental for favorable skin tissue insertion ability.[61] Additionally, FITC-labeled rhCol III and nile red@PLGA were loaded in the MN, and fluorescent pictures were taken to better display the distribution of drugs in the MN. As illustrated from Fig. 2E and F, drugs were distributed on the tips and base of the MN.

In order to verify whether the prepared MN can penetrate the skin tissue to deliver the drug to the dermis effectively, the mechanical properties of the MN were measured using a universal testing machine. Firstly, as shown in Fig. S4A,† the MN

was fixed on a flat surface with the tip facing upward. Subsequently, the forced experiment started when the mechanical sensor touched the tips of MN and lasted until it traveled 400 μm at a controlled speed of 100 μm s^{-1} (Fig. S4B and C†). Fig. 2G showed the profiles of the failure force against the displacement. The force increased with the displacement after the needle tips contacted the probe. There were no discontinuous points detected, indicating that MN would bend but not break. After 400 μm of displacement, the average forces required to bend MN-C and MN-III (6.22–7.31 N) were higher than those for MN-Nap and MN-III/Nap (3.98–5.72 N). As illustrated in Fig. S5,† the mechanical strength of MN showed an obvious downward trend as the concentration of nanoparticles increased. These results demonstrated that the addition of Nap@PLGA nanoparticles weakened the mechanical strength of the MN to a certain extent. However, it has been reported that the insertion force of individual MN into human skin varied from 0.1 to 3.0 N without breaking.[62] Therefore, considering the above-mentioned data, the as-prepared MNs could enable skin tissue puncture and insertion. Then, the skin insertion ability of MN-III/NAP was studied by the trypan blue staining method. After inserting MN, an array of pinholes appeared on the surface of the skin (Fig. 2H and I), and a consistent blue microchannel was observed through an optical microscope (Fig. S6†), indicating that the MN-III/NAP could penetrate the skin. In addition, the FITC-labeled rhCol III-loaded MN could be easily inserted into the rat's back skin to form microchannels (Fig. 2J). According to fluorescence microscope images (Fig. 2K and L), FITC-labeled rhCol III remained in the microchannel of the rat's back skin, which further proved that the prepared MN could penetrate the skin.

3.3 Proliferation and scratch healing of L929 cells

The basic qualities of well-designed biomaterials are favorable biocompatibility and non-cytotoxicity.[63] Here, the viability of L929 fibroblast cells, which played a vital role in the progress of wound healing was employed to assess the cytocompatibility of MNs.[2] The results of CCK8 assays are illustrated in Fig. 3A. Compared with the control group (without MN solution treatment), there was a noticeable growth trend of L929 cells proliferation of all MN groups, indicating that all prepared MNs possessed good biocompatibility. The cell activity of the MN-III and MN-Nap/III groups was remarkably higher than that of the control, MN-C and MN-Nap groups. In addition, as illustrated in Fig. 3B, the results of cells fluorescence staining were also in keeping with the quantitative CCK-8 assay. After 24 or 48 h incubation, the living L929 cells which were stained green displayed a spindle-like morphology in all groups, indicating that the cells grew well. Importantly, the fluorescence intensity of MN-III and MN-III/Nap groups was significantly stronger than that in the other three groups, indicating that MN containing rhCol III could significantly enhance the proliferation of L929 cells.

Furthermore, in order to research the influence of MNs on the migration of L929 cells, scratched cells were imaged at 0, 24 and 48 h. As shown in Fig. 3C and D, the growth and migration of L929 cells in MN-III and MN-III/Nap groups were faster than those in the control group. There was an obvious difference between the healing area in the MN-III/Nap group and the MN-C groups at each time point. At 48 h, the percentage of scratch closure area reached around 90% for the MN-III and MN-III/Nap groups (Fig. 3C), while the scratch closure area for the MN-C group was less than 50%. These

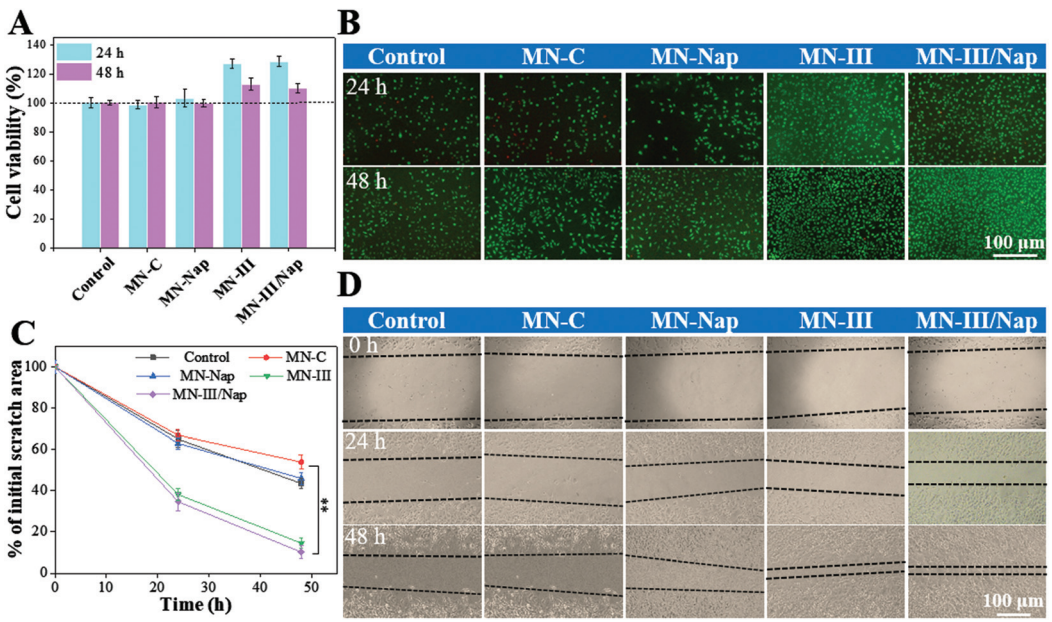

Fig. 3 Cell viability (A) and live/dead staining (B) of L929 cells after incubation with MN solution for 24 h and 48 h. The quantitative analysis (C) and pictures (D) of the cell wound scratch assay of L929 cells at different times. *P < 0.01, **P < 0.001.

results showed that MN containing rhCol III could accelerate the L929 cells scratch healing. Taken together, MN-III/Nap not only possessed good biocompatibility but also had a positive effect on L929 cells proliferation and migration, indicating it possessed the potential to facilitate wound healing.

3.4 Proliferation and scratch healing of HUVECs

Angiogenesis is a dynamic process and is critical for successful wound healing, while the proliferation and migration of endothelial cells are very important for angiogenesis.[64] Firstly, CCK8 assays and live/dead staining were used to evaluate the effects of MNs on the proliferation of HUVECs. As illustrated in Fig. S7A,† after 48 h incubation, cell viability of MN-III and MN-III/Nap groups were 112% and 117%, respectively, which were higher than those of the control group. In addition, the results of live/dead staining showed that fluorescence intensities of MN-III and MN-III/Nap groups were significantly stronger than the control group (Fig. S7B†). It is proposed that the higher vitality of HUVECs might be attributed to the addition of rhCol III with strong cell adhesion.

In order to evaluate the ability of MNs to promote migration of HUVECs, *in vitro* wound scratch assay was performed and the results are shown in Fig. S7C and D.† As illustrated in Fig. S7D,† the scratched area of HUVECs treated with MN containing rhCol III closed faster during 48 h of incubation compared to the control group. Furthermore, as shown in Fig. S7C,† the quantitative results analyzed using ImageJ software indicated that the cell scratch coverage reached 82% and 79% after 48 h of incubation with MN-III and MN-III/Nap, respectively. While the cell scratch coverage in control and MN-C groups reached 50% and 49%, respectively. The *in vitro* wound scratch assay demonstrated that rhCol III-loaded MNs could effectively promote the migration of HUVECs, indicating that rhCol III-loaded MNs possessed a positive effect on the formation of neovascularization after injury.

3.5 Wound healing *in vivo*

Results from the *in vitro* study revealed that Nap@PLGA and rhCol III co-loaded MN possessed synergistic effects of reducing inflammation and promoting cell migration and proliferation. To evaluate treatment effects and application prospects of the MN-III/Nap *in vivo* wound healing, diabetic rats were divided into five groups including control (injury without any treatment), MN-C (injury and treated with unmodified MN), MN-III (injury and treated with rhCol III-loaded MN), MN-Nap (injury and treated with Nap loaded MN) and MN-III/Nap (injury and treated with Nap@PLGA and rhCol III co-loaded MN) groups, for the establishment of skin wound model.

Digital photos of wounds at days 0, 2, 4, 7 and 14 were recorded and wound closure was calculated based on wound size relative to the initial wound dimensions (Fig. 4A and B). As shown in Fig. 4B, during the hemostasis phase, the self-contraction of the wound could lead to a partial closure of the skin epidermis. Subsequently, with the formation of epidermis, the wound area of all MN-treatment groups gradually decreased. All groups showed a certain degree of wound contraction on the 2nd day. The MN-III/Nap group displayed the largest wound closure rate of 41.36 ± 1.43%, which illustrated the MN-III/Nap group possessed a relatively higher promotion effect on wound healing. After 4 days of treatment, the wound closure rates of the control, MN-C, MN-III, MN-Nap and MN-III/Nap were 15.28 ± 1.47%, 30.33 ± 0.37%, 55.14 ± 1.50%, 47.37 ± 2.96% and 58.39 ± 1.85%, respectively (Fig. 4B). It was worth mentioning that wounds in the MN-III /Nap group showed an obvious epidermal regeneration on the 4th day. Subsequently, the wound area of each group was further reduced on the 7th day. After 14 days of treatment, MN-III/Nap-treated wounds were almost healed and covered with hair, illustrating that MN-III/Nap possessed an excellent effect on promoting wound healing. The corresponding average wound closure rate was 98.83 ± 0.36%, while the wound closure rate of the control group was only 70.36 ± 3.95%. As illustrated above, the MN-III/Nap group possessed a better healing effect on diabetic wounds.

3.6 Histological evaluation in wound healing

Furthermore, for the purpose of evaluating collagen deposition, inflammatory reactions, tissue regeneration and angiogenesis in the wound healing process and after 7 days and 14 days of MN treatment, histological analysis was performed. Firstly, H&E was used to stain tissues of wounds and inflammatory cells, which infiltrated the wound site.[65] As shown in Fig. 4C, on the 7th day, numerous lymphocytes and red blood cell infiltration could be observed in the wound site treated with MN-C, illustrating the serious inflammatory reaction at the wound site. In contrast, there were insignificant lymphocytes observed in the MN-III/Nap group, indicating that MN-III/Nap could remarkably decrease the level of inflammation within 7 days to accelerate epidermal remodeling. After 14 days of treatment, the wounds developed the fundamental structure of epithelium and dermis except for the control group and MN-C group. In addition, the wound for the control or MN-C group was not completely filled. Moreover, the regulation of epithelium and connective tissue in the MN-III/Nap group was higher than that in the control and MN-C groups. There were more fibroblasts, more blood vessels and hair follicles in the MN-III/Nap group than those in other groups. These results demonstrated the MN-III/Nap possessed the best healing effect.

Collagen deposition plays a critical role in the functional reconstruction of diabetic wounds.[66] Specifically, collagen is continuously synthesized by active fibroblasts and serves as a template for new tissue growth in the proliferation stage during wound repair. Moreover, the deposited collagen is associated with the strength of the new tissue in the mature stage of wound healing.[67,68] Consequently, the amount of collagen deposition is one of the most important indicators to evaluate the effect of wound repair. Here, Masson staining was used to detect the deposition and appearance of new collagen on day 7 or day 14 after surgery. As illustrated in Fig. 4D, in the neonatal skin tissue structure of the MN-III/Nap group, there was a large number of regenerated collagen fibers that could be observed on the 7th day after surgery. The completely

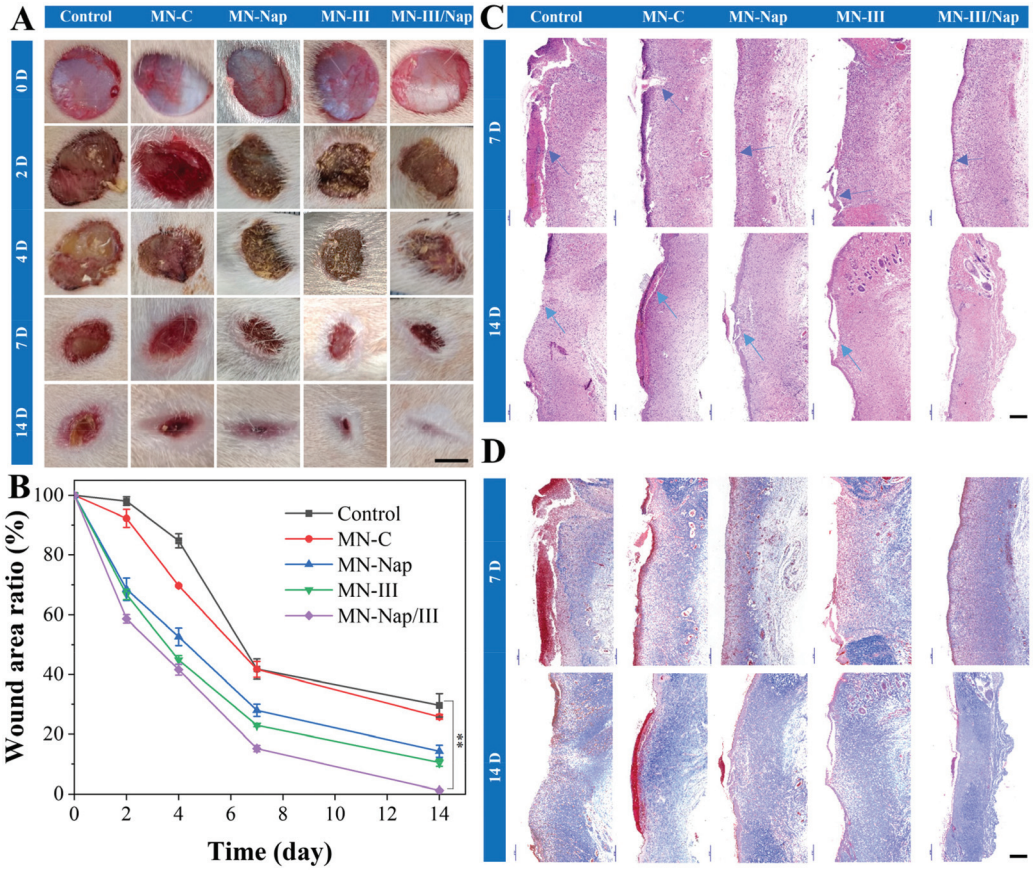

Fig. 4 Analysis of the treatment effect of the full-thickness skin wounds of a type I diabetes rat model. (A) Digital images of wounds and the wound area ratio (B) at different times during the 14 D *in vivo* treatment (mean ± SD, n = 6), *P < 0.01, **P < 0.001. The scale bar was 0.6 cm. H&E staining (C) and Masson's staining (D) of tissue sections at 7 D and 14 D. The scale bar is 500 μm.

regenerated epithelial tissue was also seen in the MN-III/Nap group. On the 14th day after surgery, although new collagen deposition and regenerated tissue formation appeared in all groups, the collagen deposition in the MN-III/Nap group far exceeded the control group or MN-C group with regular orientation and evenly distribution. These results illustrated that the MN-III/Nap could promote the diabetic wound healing process by accelerating fibroblast cell migration and proliferation, granulation tissue formation and collagen deposition with the formation of mature epithelial structures.

3.7 CD68 and CD31 expression during wound healing

When trauma occurs, inflammation, a spontaneous self-defense mechanism of the human body against environmental stimuli, is inevitable.[2,6] Although an appropriate inflammatory response is favorable for the healing process of a skin wound, excessive inflammation may impede wound repair. Here, fluorescent immunohistochemical staining for CD68 was conducted to evaluate the effects of MN-III/Nap on skin inflammation during the wound healing process. As illustrated in Fig. 5A, the expression of CD68 in the MN-III/Nap group was remarkably lower than that in control and MN-C groups. Quantitative analysis results of macrophage cells are shown in Fig. 5B. The number of macrophage cells in MN-III/Nap, MN-C and control groups were 399 ± 20, 915 ± 13 and 1021 ± 16, respectively. Plenty of inflammatory cells aggregated in the wound site in MN-C and control groups, which illustrated that the inflammation was not fully treated, while fewer inflammatory cells infiltration were observed around the wound in the MN-III/Nap group, which was due to the good anti-inflammatory effect of the released Nap. Subsequently, on the 14th day, the number of macrophage cells decreased to 152 ± 18 in the MN-III/Nap group, 422 ± 21 in the MN-C group and 514 ± 14 in the control group. These results suggested that MN-III/Nap could effectively alleviate the local inflammatory reaction during diabetic wound healing applications.

It is well known that the vascular network plays a key role in the regeneration/repair of full-thickness skin for its function of transporting nutrients, oxygen, and infiltration of immune cells to the wound area.[42] The platelet endothelial cell adhesion molecule-1 (CD31), which is a typical biomarker of vascular endothelial differentiation, can act as an indicator of the degree of vascularization during wound healing process.[69,70] Therefore, in this study, the newly formed blood vessels were evaluated using immunohistochemical staining of CD31. As shown in Fig. 5C, the positive-stained endothelial

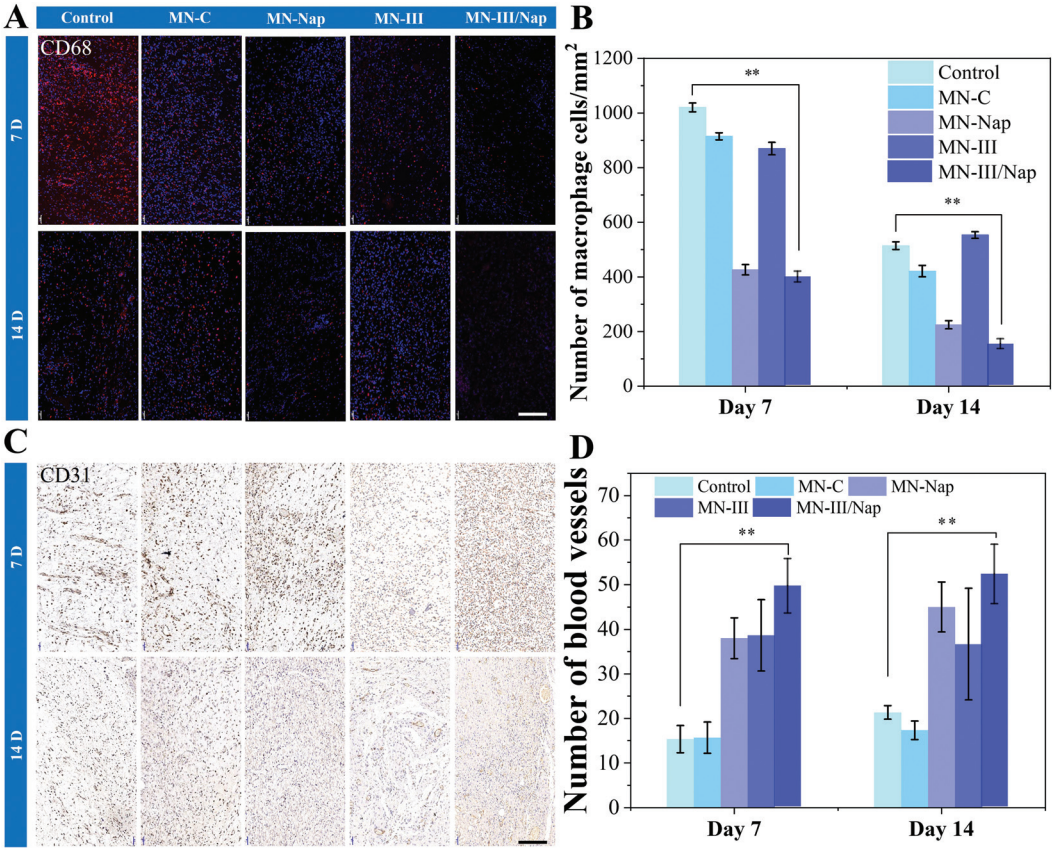

Fig. 5 (A) Fluorescent immunohistochemical analysis of regenerated tissues at wound sites with CD68 (local macrophages) staining. Scale bar = 200 μm. (B) Quantitative analysis of macrophage cells in the wound sites. (C) Immunohistochemical staining of CD31 of sections at days 7 and 14. Scale bar = 200 μm. (D) The number of newly formed blood vessels was measured from the immunohistochemical images. *P < 0.01, **P < 0.001.

cells arranged in a liner or a closed-loop shape could be identified as a blood vessel and the number of blood vessels in each wound was calculated from Fig. 5D. For the control group, capillaries were mostly round and relatively small in diameter, and their growth mode was non-budding during wound repair. As for the MN-III/Nap group, most of the new capillaries were flat, linear and large in area, which was budding growth. In addition, the number of newly formed blood vessels after 7 days of treatment in the MN-III/Nap group was 49 ± 6, which was remarkably higher than that in control (15 ± 3) and MN-C groups (21 ± 2) (Fig. 5D). Furthermore, after 14 days of treatment, the number of newly formed blood vessel in control, MN-C and MN-III/Nap groups was 21 ± 1, 17 ± 2 and 52 ± 7, respectively, illustrating that the prepared MN-III/Nap possessed the function of promoting the regeneration of new blood vessels in the healing process of the diabetic wound.

4. Conclusions

In this work, we developed a novel MN patch, called the MN-III/Nap, for the treatment of diabetic chronic wounds covered by crust and necrotic tissue. To our best knowledge, it was the first dressing to utilize an MN patch to facilitate local delivery of rhCol III in a minimally invasive way. The dissolving MN-III/Nap was fabricated by a template-molding method. The array of the prepared MN showed excellent mechanical integrity with a strength of 3.98–5.72 N, which was sufficient to penetrate the tissue barrier at the wound site. *In vitro* cell culture results showed that rhCol III-loaded MNs could effectively enhance the proliferation and migration of fibroblasts and endothelial cells. Additionally, the full-thickness skin wounds of a type I diabetes rat model was used to verify the *in vivo* therapeutic efficacy of the MN-III/Nap. Compared with the control group, the MN-III/Nap could effectively alleviate the local inflammatory reaction of the tissue around the wound site. Importantly, the MN-III/Nap-treated wounds showed a faster wound closure rate, improved epithelialization, more collagen deposition and relatively complete CD31-positive microvasculature. These favorable characteristics indicated that rhCol III and Nap-loaded MNs were expected to be potential candidates for diabetic wound healing, and proved the huge application potential of rhCol III in wound dressings.

Conflicts of interest

All authors declare that they have no conflict of interest.

Acknowledgements

This work is supported by National Natural Science Foundation of China (32101107), National Key Research and Development Programs (2017YFC1104200), the Program of Introducing Talents of Discipline to Universities (111 Project, No. B16033), the Fundamental Research Funds for the Central Universities (No. YJ2021115) and the 1·3·5 project for disciplines of excellence, West China Hospital, Sichuan University (ZYJC21026, ZYJC21077).

References

1 H. S. Kim, X. Sun, J. H. Lee, H. W. Kim, X. Fu and K. W. Leong, *Adv. Drug Delivery Rev.*, 2019, **146**, 209–239.
2 S. Saghazadeh, C. Rinoldi, M. Schot, S. S. Kashaf, F. Sharifi, E. Jalilian, K. Nuutila, G. Giatsidis, P. Mostafalu, H. Derakhshandeh, K. Yue, W. Swieszkowski, A. Memic, A. Tamayol and A. Khademhosseini, *Adv. Drug Delivery Rev.*, 2018, **127**, 138–166.
3 S. Sharifi, M. J. Hajipour, L. Gould and M. Mahmoudi, *Mol. Pharm.*, 2020, **18**, 550–575.
4 B. K. Sun, Z. Siprashvili and P. A. Khavari, *Science*, 2014, **346**, 941–945.
5 A. P. Veith, K. Henderson, A. Spencer, A. D. Sligar and A. B. Baker, *Adv. Drug Delivery Rev.*, 2019, **146**, 97–125.
6 M. Ashtikar and M. G. Wacker, *Adv. Drug Delivery Rev.*, 2018, **129**, 194–218.
7 K. Las Heras, M. Igartua, E. Santos-Vizcaino and R. M. Hernandez, *J. Controlled Release*, 2020, **328**, 532–550.
8 H. Kuivaniemi and G. Tromp, *Gene*, 2019, **707**, 151–171.
9 C. Hua, Y. Zhu, W. Xu, S. Ye, R. Zhang, L. Lu and S. Jiang, *Biochem. Biophys. Res. Commun.*, 2019, **508**, 1018–1023.
10 K. Gelse, E. Pöschl and T. Aigner, *Adv. Drug Delivery Rev.*, 2003, **55**, 1531–1546.
11 C. H. Lee, A. Singla and Y. Lee, *Int. J. Pharmaceut.*, 2003, **55**, 1531–1546.
12 J. N. Clore, I. K. Cohen and R. F. Diegelmann, *Proc. Soc. Exp. Biol. Med.*, 1979, **161**, 337–340.
13 M. Makuszewska, T. Bonda, M. Cieślińska, I. Bialuk, M. M. Winnicka and K. Niemczyk, *Int. J. Pediatr. Otorhinolaryngol.*, 2020, **136**, 110196.
14 X. Liu, H. Wu, M. Byrne, S. Krane and R. Jaenisch, *Proc. Natl. Acad. Sci. U. S. A.*, 1997, **94**, 1852–1856.
15 L. E. Tracy, R. A. Minasian and E. J. Caterson, *Adv. Wound Care*, 2016, **5**, 119–136.
16 D. R. Keene, L. Y. Sakai, H. P. Bachinger and R. E. Burgerson, *J. Cell Biol.*, 1987, **105**, 2393–2402.
17 S. D'hondt, B. Guillemyn, D. Syx, S. Symoens, R. De Rycke, L. Vanhoutte, W. Toussaint, B. N. Lambrecht, A. De Paepe, D. R. Keene, Y. Ishikawa, H. P. Bächinger, S. Janssens, M. J. M. Bertrand and F. Malfait, *Matrix Biol.*, 2018, **70**, 72–83.
18 E. Davison-Kotler, W. S. Marshall and E. García-Gareta, *Bioengineering*, 2019, **6**, 1–15.
19 A. Deng, Y. Yang, S. Du, X. Yang, S. Pang, X. Wang and S. Yang, *Mater. Sci. Eng., C*, 2021, **119**, 111555.
20 A. Muheem, F. Shakeel, M. A. Jahangir, M. Anwar, N. Mallick, G. K. Jain, M. H. Warsi and F. J. Ahmad, *Saudi Pharm. J.*, 2016, **24**, 413–428.
21 S. McLaughlin, B. McNeill, J. Podrebarac, K. Hosoyama, V. Sedlakova, G. Cron, D. Smyth, R. Seymour, K. Goel, W. Liang, K. J. Rayner, M. Ruel, E. J. Suuronen and E. I. Alarcon, *Nat. Commun.*, 2019, **10**, 1–14.
22 S. You, S. Liu, X. Dong, H. Li, Y. Zhu and L. Hu, *ACS Biomater. Sci. Eng.*, 2020, **6**, 1977–1988.
23 L. Yang, H. Wu, L. Lu, Q. He, B. Xi, H. Yu, R. Luo, Y. Wang and X. Zhang, *Biomaterials*, 2021, **276**, 121055.
24 A. Hardy, C. Seguin, A. Brion, P. Lavalle, P. Schaaf, S. Fournel, L. Bourel-Bonnet, B. Frisch and M. De Giorgi, *ACS Appl. Mater. Interfaces*, 2018, **10**, 29347–29356.
25 S. A. Eming, T. Krieg and J. M. Davidson, *J. Invest. Dermatol.*, 2007, **127**, 514–525.
26 C. Y. Chen, H. Yin, X. Chen, T. H. Chen, H. M. Liu, S. S. Rao, Y. J. Tan, Y. X. Qian, Y. W. Liu, X. K. Hu, M. J. Luo, Z. X. Wang, Z. Z. Liu, J. Cao, Z. H. He, B. Wu, T. Yue, Y. Y. Wang, K. Xia, Z. W. Luo, Y. Wang, W. Y. Situ, W. E. Liu, S. Y. Tang and H. Xie, *Sci. Adv.*, 2020, **6**, eaba0942.
27 G. M. Seon, M. H. Lee, M. A. Koo, S. H. Hong, Y. J. Park, H. K. Jeong, B. J. Kwon, D. Kim and J. C. Park, *Mater. Sci. Eng., C*, 2021, **121**, 111837.
28 P. Ahangar, S. J. Mills, L. E. Smith, S. Gronthos and A. J. Cowin, *npj Regener. Med.*, 2020, **24**, 1–10.
29 R. Bushra and N. Aslam, *Oman Med. J.*, 2010, **25**, 155–161.
30 C. Hu, F. Zhang, L. Long, Q. Kong, R. Luo and Y. Wang, *J. Controlled Release*, 2020, **324**, 204–217.
31 C. Akduman, I. Özgüney and E. P. A. Kumbasar, *Mater. Sci. Eng., C*, 2016, **64**, 383–390.
32 V. U. Godakanda, H. Li, L. Alquezar, L. Zhao, L. M. Zhu, R. de Silva, K. M. N. de Silva and G. R. Williams, *Int. J. Pharm.*, 2019, **562**, 172–179.
33 R. J. Van Der Vijver, C. J. Van Laarhoven, R. M. Lomme and T. Hendriks, *Int. J. Colorectal Dis.*, 2013, **28**, 1209–1216.
34 S. L. Percival, S. M. McCarty and B. Lipsky, *Adv. Wound Care*, 2015, **4**, 373–381.
35 A. C. Anselmo, Y. Gokarn and S. Mitragotri, *Nat. Rev. Drug Discovery*, 2018, **18**, 19–40.
36 M. Chen, G. Quan, Y. Sun, D. Yang, X. Pan and C. Wu, *J. Controlled Release*, 2020, **325**, 163–175.
37 D. J. Lim, J. B. Vines, H. Park and S. H. Lee, *Int. J. Biol. Macromol.*, 2018, **110**, 30–38.
38 A. J. Paredes, P. E. McKenna, I. K. Ramöller, Y. A. Naser, F. Volpe-Zanutto, M. Li, M. T. A. Abbate, L. Zhao, C. Zhang, J. M. Abu-Ershaid, X. Dai and R. F. Donnelly, *Adv. Funct. Mater.*, 2021, **31**, 1–27.
39 R. S. J. Ingrole, E. Azizoglu, M. Dul, J. C. Birchall, H. S. Gill and M. R. Prausnitz, *Biomaterials*, 2021, **267**, 120491.
40 Y. Zhang, J. Yu, A. R. Kahkoska, J. Wang, J. B. Buse and Z. Gu, *Adv. Drug Delivery Rev.*, 2019, **139**, 51–70.

41 R. Huang, X. Zhang, W. Li, L. Shang, H. Wang and Y. Zhao, *Adv. Sci.*, 2021, **8**, 1–8.
42 R. Jamaledin, C. K. Y. Yiu, E. N. Zare, L. N. Niu, R. Vecchione, G. Chen, Z. Gu, F. R. Tay and P. Makvandi, *Adv. Mater.*, 2020, **32**, 1–29.
43 L. Barnum, M. Samandari, T. A. Schmidt and A. Tamayol, *Expert Opin. Drug Delivery*, 2020, **17**, 1767–1780.
44 B. Gao, M. Guo, K. Lyu, T. Chu and B. He, *Adv. Funct. Mater.*, 2021, **31**, 1–9.
45 Y. Su, V. L. Mainardi, H. Wang, A. McCarthy, Y. S. Zhang, S. Chen, J. V. John, S. L. Wong, R. R. Hollins, G. Wang and J. Xie, *ACS Nano*, 2020, **14**, 11775–11786.
46 X. Zhang, G. Chen, Y. Liu, L. Sun, L. Sun and Y. Zhao, *ACS Nano*, 2020, **14**, 5901–5908.
47 J. Chi, X. Zhang, C. Chen, C. Shao, Y. Zhao and Y. Wang, *Bioact. Mater.*, 2020, **5**, 253–259.
48 X. Yu, M. Li, L. Zhu, J. Li, G. Zhang, R. Fang, Z. Wu and Y. Jin, *Acta Biomater.*, 2020, **112**, 87–100.
49 H. Derakhshandeh, F. Aghabaglou, A. McCarthy, A. Mostafavi, C. Wiseman, Z. Bonick, I. Ghanavati, S. Harris, C. Kreikemeier-Bower, S. M. Moosavi Basri, J. Rosenbohm, R. Yang, P. Mostafalu, D. Orgill and A. Tamayol, *Adv. Funct. Mater.*, 2020, **30**, 1–11.
50 M. Samandari, F. Aghabaglou, K. Nuutila, H. Derakhshandeh, Y. Zhang, Y. Endo, S. Harris, L. Barnum, C. Kreikemeier-Bower, E. Arab-Tehrany, N. A. Peppas, I. Sinha and A. Tamayol, *Adv. Healthcare Mater.*, 2021, **2001800**, 1–11.
51 K. J. Lee, Y. Xue, J. Lee, H. J. Kim, Y. Liu, P. Tebon, E. Sarikhani, W. Sun, S. Zhang, R. Haghniaz, B. Çelebi-Saltik, X. Zhou, S. Ostrovidov, S. Ahadian, N. Ashammakhi, M. R. Dokmeci and A. Khademhosseini, *Adv. Funct. Mater.*, 2020, **30**, 1–11.
52 X. Zhang, G. Chen, L. Sun, F. Ye, X. Shen and Y. Zhao, *Chem. Eng. J.*, 2021, **406**, 126741.
53 E. Y. Jeon, J. Lee, B. J. Kim, K. Il Joo, K. H. Kim, G. Lim and H. J. Cha, *Biomaterials*, 2019, **222**, 119439.
54 M. F. P. Graça, S. P. Miguel, C. S. D. Cabral and I. J. Correia, *Carbohydr. Polym.*, 2020, **241**, 116364.
55 Y. Wang, K. Zhang, X. Qin, T. Li, J. Qiu, T. Yin, J. Huang, S. McGinty, G. Pontrelli, J. Ren, Q. Wang, W. Wu and G. Wang, *Adv. Sci.*, 2019, **19**, 1900172.
56 J. Zhuang, R. H. Fang and L. Zhang, *Small Methods*, 2017, **1**, 1700147.
57 K. K. Chereddy, R. Coco, P. B. Memvanga, B. Ucakar, A. Des Rieux, G. Vandermeulen and V. Préat, *J. Controlled Release*, 2013, **171**, 208–215.
58 M. Berthet, Y. Gauthier, C. Lacroix, B. Verrier and C. Monge, *Trends Biotechnol.*, 2017, **35**, 770–784.
59 U. Angkawinitwong, A. J. Courtenay, A. M. Rodgers, E. Larrañeta, H. O. Mccarthy, S. Brocchini, R. F. Donnelly and G. R. Williams, *ACS Appl. Mater. Interfaces*, 2020, **12**, 12478–12488.
60 C. Hu, W. Zhuang, T. Yu, L. Chen, Z. Liang, G. Li and Y. Wang, *J. Mater. Chem. B*, 2020, **8**, 5267–5279.
61 D. F. S. Fonseca, C. Vilela, R. J. B. Pinto, V. Bastos, H. Oliveira, J. Catarino, P. Faísca, C. Rosado, A. J. D. Silvestre and C. S. R. Freire, *Mater. Sci. Eng., C*, 2021, **118**, 111350.
62 M. R. Prausnitz, *Adv. Drug Delivery Rev.*, 2004, **56**, 581–587.
63 Z. Feng, Q. Su, C. Zhang, P. Huang, H. Song, A. Dong, D. Kong and W. Wang, *Adv. Funct. Mater.*, 2020, **30**, 1–13.
64 J. Gu, Q. Zhang, M. Geng, W. Wang, J. Yang, A. ur R. Khan, H. Du, Z. Sha, X. Zhou and C. He, *Bioact. Mater.*, 2021, **6**, 3254–3268.
65 B. Yang, J. Song, Y. Jiang, M. Li, J. Wei, J. Qin, W. Peng, F. L. Lasaosa, Y. He, H. Mao, J. Yang and Z. Gu, *ACS Appl. Mater. Interfaces*, 2020, **12**, 57782–57797.
66 J. Liu, R. Huang, G. Li, D. L. Kaplan, Z. Zheng and X. Wang, *Biomacromolecules*, 2021, **22**, 546–556.
67 L. Wang, X. Zhang, K. Yang, Y. V. Fu, T. Xu, S. Li, D. Zhang, L. N. Wang and C. S. Lee, *Adv. Funct. Mater.*, 2020, **30**, 1–14.
68 Y. Liang, B. Chen, M. Li, J. He, Z. Yin and B. Guo, *Biomacromolecules*, 2020, **21**, 1841–1852.
69 M. Li, Y. Liang, J. He, H. Zhang and B. Guo, *Chem. Mater.*, 2020, **32**, 9937–9953.
70 Y. Chen, Y. Liang, J. Liu, J. Yang, N. Jia, C. Zhu and J. Zhang, *Biomater. Sci.*, 2021, **9**, 238–251.